Determination of the line emission locations in a large helical device on the basis of the Zeeman effect

M. Goto and S. Morita
National Institute for Fusion Science, Toki 509-5292, Japan
(Received 11 June 2001; published 3 January 2002)

Neutral helium He I λ 728.1 nm ($2\,^1P$-$3\,^1S$) and λ 667.8 nm ($2\,^1P$-$3\,^1D$) emission lines have been observed with an array of optical fibers that cover the entire poloidal cross section of the plasma. The Zeeman profile yields a magnetic field strength, and the locations of the emission regions are identified on the well-established map of the magnetic field of the plasma. It is found that the emission region forms a closed zone just outside the region, the so-called ''ergodic layer,'' where the magnetic field line structure is chaotic. A collisional-radiative model calculation for an inward atom flux suggests a peaked emission profile of about 3.5 cm in full width at half maximum, and this is consistent with the experimental result. The inward atom flux is found to decay before reaching the last closed flux surface and this implies a screening effect of the ergodic layer.

DOI: 10.1103/PhysRevE.65.026401 PACS number(s): 52.55.−s

I. INTRODUCTION

In fusion devices such as tokamaks and helical machines, determination of neutral particle influx from the plasma edge region to the main plasma is extremely important for the purpose of studying, e.g., the *H* mode [1,2] and the formation of density profiles [3]. In this regard, the emission line intensity is the only source of information. In conventional spectroscopy, we measure the intensity of an emission line that is integrated over the line of sight. When we can assume, say, cylindrical symmetry, we can convert the measured chord dependence of the emission line intensities to the radial distribution of the intensity. Even in the case that we can assume cylindrical symmetry for the plasma, however, this may not be the case for the neutral atom influx, because the distribution of the neutral atoms depends on the structure of the plasma vessel and on the operation of the plasma. For plasma with a large noncircular shape like divertor-configuration tokamaks and helical devices, the cylindrical symmetry is not valid even for the plasma. We thus seek to develop a method to determine the local intensities from the line integrated emission intensity. One candidate for such a method is to use the Zeeman splitting of spectral lines. Work in this direction on Alcator *C*-Mod tokamak device has been reported recently [4,5]. In the following, we report our attempt on a helical device.

II. EXPERIMENT AND ANALYSIS

Large helical device (LHD) is a heliotron type device of a double null divertor configuration [6]. The major and averaged minor radii are 3.5–3.9 m and 0.54–0.64 m, respectively. Because of the absence of inductive current, the magnetic field is determined accurately by coil currents. The maximum magnetic field strength on the magnetic axis B_{ax} could be as high as 3 T. The field structure is saddle shaped and the field strength near the helical coils is at least twice as high as the lowest field near the *X* points (see Fig. 1). In the confinement region the field lines form closed magnetic surfaces and the outermost surface is called the last closed flux surface (LCFS). Outside the LCFS both ends of the field lines are connected to the divertor plates and generally the length of the field lines are only several meters. In a region having a thickness of several centimeters just outside the LCFS the magnetic field has a chaotic structure and the field line through the layer often has a length of several kilometers [7,8]. This region is called the ''ergodic layer.'' As a result, in this layer there forms a plasma, the parameters of which are high enough to ionize neutral atoms (see Fig. 8 later). Once the atoms are ionized, they are trapped by the magnetic field and guided to the divertor plates unless they diffuse out or become neutral again by charge exchange processes. Thus this layer reduces the fueling efficiency [9] by preventing neutral atoms from penetrating into the core region.

Emission from the LHD plasma was observed with a set of parallel optical fibers, the lines of sight of which cover the entire cross section of the plasma that is elongated in the major radial direction as shown in Fig. 1. Each line of sight is collimated by a lens to have a cylindrical shape of about

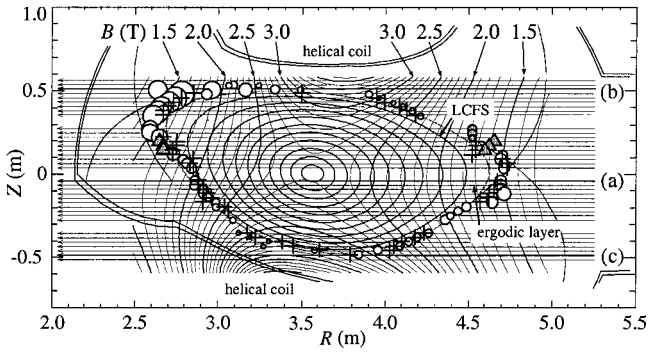

FIG. 1. Map of the magnetic surfaces and field strength for the configuration of R_{ax} =3.6 m and B_{ax} =2.75 T. The *R* and *Z* axes indicate the major radial direction and the direction perpendicular to the equatorial plane, respectively. Viewing chords are shown with the arrows. The circles and the triangles indicate the location of λ 728.1 nm line emission and their size indicates the intensity of the emission. The meanings of the details of the symbols are explained in the text. The crosses are for λ 667.8 nm.

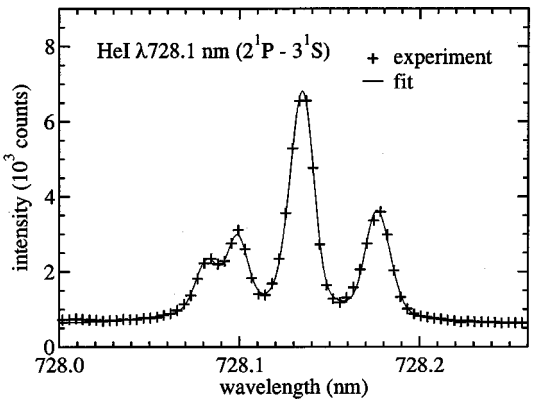

FIG. 2. Emission line profile of He I λ 728.1 nm ($2\,^1P$–$3\,^1S$) observed with the viewing chord (a) in Fig. 1. The solid line is the result of the least-squares fitting with two sets of Zeeman profiles plus a broad Gaussian profile.

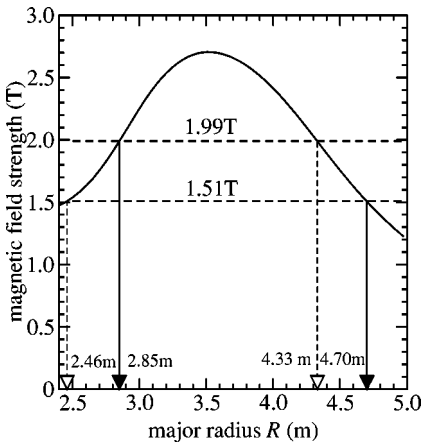

FIG. 3. Variation of magnetic field strength along the viewing chord (a) in Fig. 1. The field strengths derived from the line profile for this viewing chord are shown with the horizontal dashed lines. The identified radial positions are shown with the vertical solid lines with arrows.

30 mm diameter. Optical fibers of 5 m length guide the collected UV and visible light to a 1.33 m Czerny-Turner-type spectrometer (McPherson Model 209) having a 1800 grooves/mm grating. The end surfaces of the fibers are aligned along the entrance slit of the spectrometer such that chord-resolved spectra are recorded on a charge-coupled device detector.

The measurement was carried out for a 20 s stationary phase of a helium discharge heated by a neutral beam injection (NBI) of 25 s pulse duration. The nominal field strength B_{ax} and the radius of the magnetic axis R_{ax} of the discharge were 2.75 T and 3.6 m, respectively. The actual field strength at the plasma center in this cross section was 2.67 T. The NBI power was 1.2 MW. The gas-fueling rate was controlled so as to keep the line-averaged electron density $\overline{n_e}$, constant. In the stationary phase $\overline{n_e}$ and the electron temperature at the plasma center were 3×10^{19} m^{-3} and 2 keV, respectively.

Figure 2 shows an example of the observed profiles of the He I λ 728.1 nm ($2\,^1P$-$3\,^1S$) line obtained on the viewing chord (a) in Fig. 1. Though this line is subjected to the normal Zeeman effect since the transition is between the singlet terms, the observed profile shows a rather complicated structure. This profile can be understood as the superposition of two Zeeman profiles that originate from different locations on the same viewing chord and are relatively shifted.

In the normal Zeeman effect the unit of the energy level shift ΔE is expressed as [10]

$$\Delta E=\mu_B B, \tag{1}$$

where μ_B and B are the Bohr magneton and the magnetic field strength, respectively. The wavelength shift of the σ component relative to the unshifted π component $\Delta\lambda$ is then given as

$$\Delta\lambda=\frac{hc}{E_0}\frac{\Delta E}{E_0\pm\Delta E}\frac{1}{n_s}\simeq\lambda_0\frac{\Delta E}{E_0}, \tag{2}$$

where λ_0 and E_0 are the wavelength and the transition energy of the central π component, respectively, and h, c, and n_s (≈1) are Planck's constant, the speed of light, and the refractive index of air, respectively. Since the viewing chord is almost perpendicular to the direction of the magnetic field, each Zeeman profile consists of one π component and two half-amplitude σ components that are symmetrically shifted from the π component. The total angular momentum quantum number of the upper level is zero, so that the possibility of gross polarization, or a difference in the intensities of the π and σ components, is absent. This fact is favorable in reducing the uncertainty in fitting the line profile. Under these constraints we perform a least-squares fitting for the observed profile in Fig. 2 with two sets of Zeeman profiles (six Gaussian profiles) plus a broad Gaussian profile. Each profile has an independent amplitude, width, and center wavelength. The result is shown in Fig. 2 with the solid line. In this case, the broad Gaussian component has the full width at half maximum (FWHM) of 0.12 nm that corresponds to the Doppler temperature of 19 eV, and constitutes about 24% of the total intensity. The derived field strength values from the sharp Zeeman profiles are $B=1.99$ T and 1.51 T. The uncertainties are less than 0.01 T. The relative shift is 5.0×10^{-3} nm. The variation of the field strength along the viewing chord is shown in Fig. 3. Here, the above derived field strength values are indicated with horizontal dashed lines. Each of the values has two candidates for the spatial location. Candidates $R=2.46$ m for $B=1.51$ T and $R=4.33$ m for $B=1.99$ T are discarded because the former position is too far from the plasma boundary and the latter is deep inside the main plasma (see Fig. 1). We thus conclude $R=4.70$ m for the former and $R=2.85$ m for the latter. The result of this identification is shown in Fig. 1 with the open circles. In a similar analysis for all the viewing chords, we reach a unique identification of the positions in most cases as given in Fig. 1. However, there remains ambiguity for several viewing chords, which are indicated in Fig. 1 with the filled triangles; the two magnetic field values are too close. The filled circles indicate the derived field strength values with an uncertainty of about 0.05 T, which is due to the weak

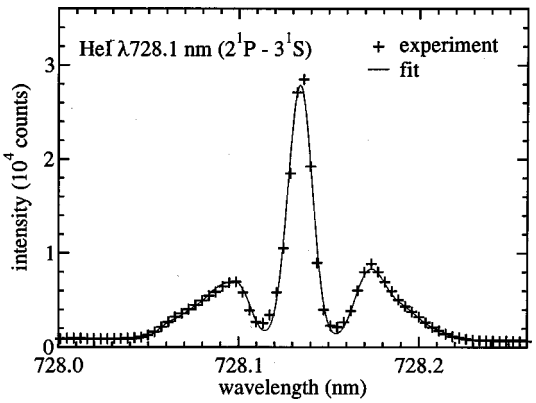

FIG. 4. Similar to Fig. 2 but with the viewing chord (b) in Fig. 1. The profile is fitted with five sets of the Zeeman profiles.

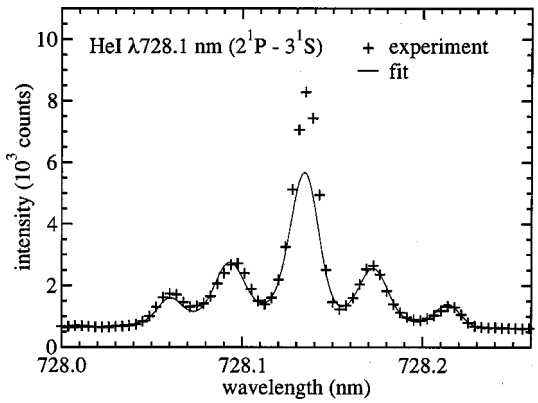

FIG. 5. Similar to Fig. 2 but with the viewing chord (c) in Fig. 1.

signals or the blending of impurity lines. The size of the symbol is proportional to the signal intensity; it is seen that very intense emissions are observed near the inner X point.

A spatial extent of the emission region could make the σ components broader than the π component. This broadening is, however, found to be smaller than 1×10^{-3} nm, or 0.05 T in most cases; this change of the magnetic field corresponds to about 5 cm around the X points, for example. An exception is the chord (b) in Fig. 1, which is nearly tangential to the outer boundary of the ergodic layer. The line profile for this chord is shown in Fig. 4. In this case the profile is fitted with five sets of Zeeman profiles, each of which has the independent amplitude, width, and center wavelength, with the field strength values from 1.4 T to 3.1 T. See Fig. 1 for the result.

In most cases a broad Gaussian component is necessary in the fitting. The temperature and the fraction of the total intensity of this component are in the range of 13–20 eV and 24–33 %, respectively. The source of this component is not positively identified but is supposed to be due to charge exchange collisions or the recombining plasma component [see Eq. (4) later]. It is noted that the temperature of helium ions, which is derived from the Doppler broadening of the λ 468.6 nm ($n=3-4$) line, is found to have similar values.

Though the λ 728.1 nm line cannot have gross polarization, some observed profiles exhibit apparent polarization. An example is shown in Fig. 5; this is obtained with the viewing chord (c) in Fig. 1 and the π component is much stronger than expected. This cannot be explained as due to an oblique viewing angle with respect to the direction normal to the magnetic field. If this were the case the apparent polarization would be opposite. The inner components of the profile correspond to the field strength of about 1.5 T, and reasonable locations cannot be found on this line of sight; the location of this field strength falls outside the vacuum vessel or far away from the plasma boundary. Rather, this component is identified as light reflected by the wall surface. For specular reflection the incident angle to the wall surface is larger than 65° so that the reflection efficiencies are expected to be different for the two polarized components; suggesting a higher efficiency for the *s*-polarized component than for the *p*-polarized component. The anomaly of the intensity ratio could be explained by this, but the complicated plasma vessel geometry prevents us from identifying the source of the reflected light.

We conducted similar measurements with the He I λ 667.8 nm ($2\,^1P$-$3\,^1D$) line. The description is almost the same as for the λ 728.1 nm line. We did not detect any gross polarization except for the reflected light. The result is shown in Fig. 1 with the crosses. The emission locations of these two lines almost coincide with each other. The slight differences would be due mainly to the slightly different conditions of the plasma.

Figure 6 shows the relative speed of the atoms that is obtained from the two Zeeman profiles like those in Fig. 2. The emission at the smaller major radius always shifts to the shorter wavelength with respect to that at the larger major radius. Unfortunately, we could not determine the absolute shift. This figure, especially the points in $Z\leqslant0$, suggests that the atoms have an inward motion with speeds of 1×10^3 to 2×10^3 m/s.

III. DISCUSSION

Figure 1 indicates that the regions of intense line emission form a closed zone, which almost coincides with the outer boundary of the ergodic layer, except for the ''dent'' at around $Z=0.05$ m, $R=2.8$ m. We do not have any explanation for this at present. As mentioned above the spatial extent

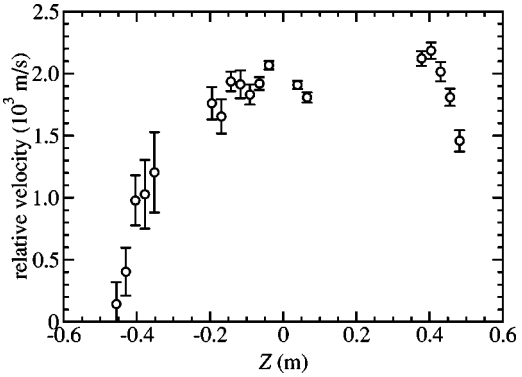

FIG. 6. Chord dependence of the apparent relative speed of the two components of atoms that is derived from the Doppler shift of the observed emission line.

of the emission region is narrower than or about 5 cm. We consider the emission intensity and the decay of the atom density in the inward atom flux by a one-dimensional model. The atom density n_{He} at the penetration depth ℓ in the x direction is expressed as

$$n_{\mathrm{He}} = n_0 \exp\left[-\int^{\ell} \frac{n_e S_{\mathrm{CR}}}{v} \mathrm{d}x \right], \tag{3}$$

where S_{CR} and v are the effective ionization rate coefficient and the penetration velocity of the atoms, respectively, and n_0 is the atom density at the edge. The ionization flux and the emission intensity for the λ 728.1 nm line, taken as an example, are expressed as $S_{\mathrm{CR}} n_e n_{\mathrm{He}}$ and $\varepsilon_{728.1} n_e n_{\mathrm{He}}$, respectively: both the quantities are defined as the number of events, ionization or photon emission, per unit volume and unit time. $\varepsilon_{728.1}$ is called the emission rate coefficient for the λ 728.1 nm line.

S_{CR} and $\varepsilon_{728.1}$ are calculated from the collisional-radiative (CR) model [11,12]. According to the CR model in which the quasi-steady-state approximation is assumed even for the metastable levels $2\,^1S$ and $2\,^3S$, the population density of excited level p is expressed as

$$n(p) = R_0(p) n_e n_{\mathrm{He}^+} + R_1(p) n_e n_{\mathrm{He}}, \tag{4}$$

where $R_0(p)$ and $R_1(p)$ are the population coefficients of the recombining and ionizing plasma component, respectively, and are functions of n_e and T_e, and n_{He^+} is the helium ion density. It may be assumed that, in the plasma peripheral region, the second term predominates over the first, at least for the sharp components of the observed profiles. In this case S_{CR} and $\varepsilon_{728.1}$ are defined as

$$\sum_{\text{all } p} S(p) n_e n(p) = \left\{ S(1) + \sum_{\text{all } p>1} S(p) R_1(p) n_e \right\} n_e n_{\mathrm{He}} \equiv S_{\mathrm{CR}} n_e n_{\mathrm{He}} \tag{5}$$

and

$$n(3\,^1S) A(3\,^1S \rightarrow 2\,^1P) = R_1(3\,^1S) n_e n_{\mathrm{He}} A(3\,^1S \rightarrow 2\,^1P) \equiv \varepsilon_{728.1} n_e n_{\mathrm{He}}, \tag{6}$$

respectively. Here, $S(p)$ is the ionization rate coefficient of level p and $A(3\,^1S \rightarrow 2\,^1P)$ is the spontaneous transition probability from $3\,^1S$ to $2\,^1P$. The level "1" stands for the ground state. Figure 7 shows the n_e dependence of the ratio $S_{\mathrm{CR}}/\varepsilon_{728.1}$ for several T_e values. It is seen that the value is rather insensitive to n_e and T_e. This means that the emission intensity could be a good measure of the ionization flux in the range of n_e and T_e shown in this figure.

By using Eq. (5) for S_{CR} we evaluate Eq. (3) numerically for positions near the outer X point on the chord (a) in Fig. 1. For n_e and T_e profiles the Thomson scattering data for a similar discharge of the same configuration are extrapolated with an exponential decay, as shown in Fig. 8. The apparent atom temperature is lower than 0.1 eV, which is the lower detection limit of the Doppler broadening. We assume a monoenergetic penetration velocity with the thermal velocity of

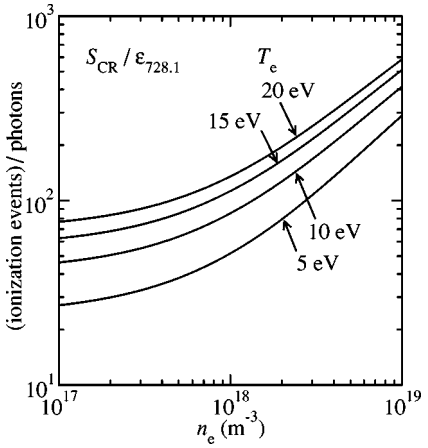

FIG. 7. n_e and T_e dependences of the ratio $S_{\mathrm{CR}}/\varepsilon_{728.1}$ calculated with the CR model under the assumption that the quasi-steady-state approximation is valid.

300 K ($v = 1.4\times10^3$ m/s). So far n_0 has not been determined yet. At the same time we calculate $\varepsilon_{728.1}$ from Eq. (6) and integrate the emission intensity over the penetration path

$$I_{728.1} = \int \varepsilon_{728.1} n_e n_{\mathrm{He}} \mathrm{d}x. \tag{7}$$

From the observed value of $I_{728.1}$ (Fig. 2) we determine n_0 to be $2.7\times10^{18}\,\mathrm{m}^{-3}$. The result is shown in Fig. 8. The spatial dependences of $\varepsilon_{728.1} n_e n_{\mathrm{He}}$ and $S_{\mathrm{CR}} n_e n_{\mathrm{He}}$ are also shown in the same figure. Both profiles have similar peaked shapes of about 3.5 cm in FWHM. This width of the emission intensity profile is consistent with the experimental result that suggests that the extent of the emission region is narrower than

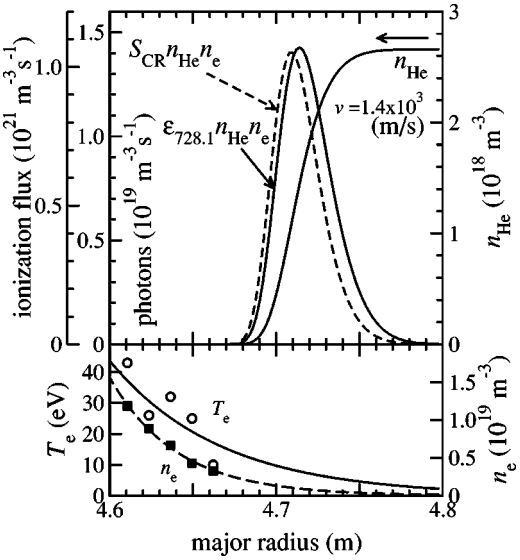

FIG. 8. Profiles of helium atom density n_{He}, emission intensity of λ 728.1 nm line $\varepsilon_{728.1} n_e n_{\mathrm{He}}$ and ionization flux $S_{\mathrm{CR}} n_e n_{\mathrm{He}}$ in a one-dimensional penetration model with the monoenergetic penetration velocity of 1.4×10^3 m/s. The n_e and T_e profiles are extrapolated exponentially from the measured values with Thomson scattering for a similar discharge.

or about 5 cm. The radial location of the emission is also in good agreement with the experiment. The atom density is found to decay in the region of strong emission intensity before reaching the LCFS, which is located at $R=4.5$ m.

We have assumed the quasi-steady-state approximation for the metastable levels. The relaxation time of the $2\,^3S$ level as determined from the ionization rate is 5×10^{-6} s for $n_e=10^{18}$ m^{-3} and $T_e=10$ eV. During this time the atoms travel 0.7 cm, short enough compared with the scale length of the plasma.

If the penetration velocity were twice the above assumption, the peaks of the emission intensity and the ionization flux would shift by 1 cm to the inward direction and become broader by 10%. Since the atom density n_0 normalized from Eq. (7) decreases by 40%, the inward particle flux $n_{\mathrm{He}}v$ and the total ionization flux $\int S_{\mathrm{CR}} n_e n_{\mathrm{He}} dx$ increase by 20%. This is caused by the n_e and T_e dependences of the ratio $S_{\mathrm{CR}}/\varepsilon_{728.1}$.

Since the neutral atom densities in the light-emitting region and in the outer region are appreciable, the opacity effects may not be neglected; we consider the effect of absorption of the resonance line, He I λ 58.4 nm ($1\,^1S$-$2\,^1P$). Since the magnetic field strength varies over space, the σ components would be optically thin throughout, and only the π component may have a significant optical thickness. On the assumption of thermal Doppler broadening with a temperature of 300 K, the absorption coefficient at the line center is about 30 m^{-1}. In the light-emitting region of several centimeters thickness (Fig. 8), the line is barely optically thick, and the effective reduction of the transition probability may be expressed in terms of the escape factor reducing the transition probability by a factor of 2 [11]. If we average the effect on the π component with the σ components, the effect of opacity on the transition probability ($[1/2+1+1]/3$) and thus on the excited-level populations (except perhaps for the $2\,^1P$ population) would be minimal. The helium gas in the outer region may be illuminated by the resonance line from the light-emitting region, again only by the π component, and the $2\,^1P$ atoms may be produced there. However, electron temperature and density there are low (see Fig. 8), and further excitation may be minimal, again.

We observed other neutral helium lines; the wavelength of the λ 501.6 nm ($2\,^1S$-$3\,^1P$) line is rather short and the Zeeman splitting is found to be too small for a similar analysis. For triplet lines the fine structure levels of the $2\,^3P_J$, for example, have the intrinsic energy level separation of $J=2$ to $J=0,1$ of about 1 cm^{-1} and this is of the same order as the Zeeman shifts for these levels under the field strength of the present experiment; $\mu_B B\simeq 1$ cm^{-1} for $B=2$ T. This makes the profiles of the λ 706.5 nm ($2\,^3P$-$3\,^3S$) and the λ 587.6 nm ($2\,^3P$-$3\,^3D$) lines complicated and a similar analysis is difficult. For the other triplet line λ 388.9 nm ($2\,^3S$-$3\,^3P$) the wavelength is too short. Even for the second-order light of the λ 388.9 nm line the splitting is found to be small; substituting Eq. (1) and $E_0=hcn_s/\lambda_0$ ($n_s\approx1$) into Eq. (2) we obtain a relation

$$\Delta\lambda \simeq \lambda_0^2 \frac{\mu_B B}{hc}, \tag{8}$$

and it is found that $\Delta\lambda$ is proportional to λ_0^2. This means the Zeeman splitting for the second-order light of the λ 388.9 nm line is about half of that for the first-order light for the λ 728.1 nm line.

Welch *et al.* observed a wavelength shift of the Zeeman split Balmer-α line of deuterium atoms in Alcator *C*-Mod [5]. They identified the Doppler shifts to the different neutral atom flows along the magnetic field lines at the two locations. LHD has a magnetic field structure that differs from that of tokamaks and has a rather thick ergodic layer outside the LCFS. We may thus conclude that, in our case, the atoms have inward motion with the thermal speed of 1×10^3 to 2×10^3 m/s. The relative speeds in Fig. 6 on the chords $0.4\,\mathrm{m}\leqslant Z\leqslant 0.5$ m do not fit in this picture; i.e., they appear too large when compared with those at $Z\simeq -0.4$ m. This is probably due to an atom flow structure resulting from the complicated geometry of the plasma vessel.

Finally, similar measurements of the Balmer-α line of hydrogen were also attempted and we encountered difficulties in fitting of the observed profile. The reasons are: (1) The wavelength λ 656.3 nm is shorter than the λ 728.1 nm, and the Zeeman splitting is smaller. The reciprocal dispersion of the spectrometer is larger by a factor of 1.08. (2) The Doppler broadening of the emission lines is larger: Hydrogen atoms have a higher temperature ($\sim$0.6 eV) than helium atoms ($<$0.1 eV) and the Doppler width becomes larger than the Zeeman splitting. Such a higher temperature of hydrogen atoms is possibly due to the existence of atoms produced from the dissociation of molecules.

ACKNOWLEDGMENTS

The support of the LHD experimental group is gratefully acknowledged. The authors are also grateful to Professor T. Fujimoto, Professor R. More, and Dr. B. J. Peterson for their critical reading of the manuscript and for their valuable advice and to Dr. T. Kobuchi for his assistance in calculating the magnetic field structure. This work was partly supported by the Ministry of Education, Culture, Sports, and Science and Technology, Japan.

[1] J.A. Snipes *et al.*, Plasma Phys. Controlled Fusion **38**, 1127 (1996).
[2] T. Fukuda, Plasma Phys. Controlled Fusion **40**, 543 (1998).
[3] S. Morita *et al.*, in *Proceedings of 16th International Conference on Fusion Energy, Montreal, 1996*, IAEA-CN-64/CP-3 (IAEA, Vienna, 1997).
[4] J.L. Weaver *et al.*, Rev. Sci. Instrum. **71**, 1664 (2000).
[5] B.L. Welch *et al.*, Phys. Plasmas **8**, 1253 (2001).
[6] O. Motojima *et al.*, Phys. Plasmas **6**, 1843 (1999).
[7] N. Ohyabu *et al.*, Nucl. Fusion **34**, 387 (1994).

[8] N. Ohyabu *et al.*, Phys. Rev. Lett. **84**, 103 (2000).
[9] S. Morita *et al.*, in *Proceedings of 26th European Conference on Controlled Fusion and Plasma Physics, Maastricht, 1999*, edited by B. Schweer, G. Van Oost, and E. Vietzke (European Physical Society, Petit-Lancy, 1999), Vol. 23J, p. 1321.
[10] P.H. Heckmann and E. Träbert, *Introduction to the Spectroscopy of Atoms* (North-Holland, Amsterdam, 1989).
[11] T. Fujimoto, J. Quant. Spectrosc. Radiat. Transf. **21**, 439 (1979).
[12] M. Goto and T. Fujimoto, National Institute for Fusion Science NIFS-DATA-43, 1997 (unpublished).